

# 1.2 Coordinate Systems

---

## 1.2.1 Introduction

One of the critical factors in the development of the AE9/AP9/SPM model was the selection of coordinate systems for mapping particle flux measurements and the binning/gridding schemes used for the maps. The empirical portion of the model requires that many individual flux measurements taken over a large extent of space and over a long time span be mapped to some reference state. This reference state must allow all the measurements to be compared and combined in a systematic way. The user of the model must then be able to map back to the reference state and retrieve the appropriate flux value and any other related quantities, such as the variance of the flux [Roederer, 1996].

There are a wide variety of coordinate systems available, each with advantages and disadvantages; see *Cabrera and Lemaire* [2007] for an excellent review. This report discusses the coordinate systems selected for AE9/AP9/SPM, their advantages and disadvantages, and their implementation. Section 1.2.2 presents some basic definitions and discusses some of the factors considered in selecting the coordinate systems. Section 1.2.3 presents the coordinate systems themselves, and Section 1.2.4 discusses the procedures used to calculate them. Appendix A attempts to provide some insight into the  $K/\Phi/h_{min}$  coordinate systems used, and Appendix B discusses transformations between coordinate systems. Appendix C provides some basic definitions of terms.

## 1.2.2 Definitions and Other Considerations

### 1.2.2.1 Adiabatic invariants

In order to account for secular variations in the Earth's magnetic field, the coordinate system chosen for AE9/AP9/SPM is based on the adiabatic invariants of trapped particle motion. The adiabatic invariants are properties of trapped particles that remain approximately constant as long as changes in external forcing factors (such as the magnetic field) vary slowly enough. The adiabatic invariants correspond to the three principal particle motions in the guiding center approximation: gyration around a field line, bounce motion along a field line, and longitudinal drift around the Earth. Conservation of the adiabatic invariants is roughly analogous to conservation of energy, mass, or angular momentum in mechanical systems. A brief discussion of the invariants is provided below.

The first adiabatic invariant  $\mu$  (called the magnetic moment) captures the particle's gyration and is defined as:

$$\mu = \frac{p_{\perp}^2}{2mB} = \frac{p^2 \sin^2 \alpha}{2mB} \quad (1)$$

where  $p$  is the particle momentum,  $m$  is the particle mass,  $B$  is the local magnetic field strength, and  $\alpha$  is the angle between the particle velocity vector and the magnetic field vector (i.e., the pitch angle).

The second adiabatic invariant  $J$ ,  $I$ , or  $K$  captures the particle's bounce motion:

$$J = 2 \int_{l_1}^{l_2} mv_{\parallel} dl \quad (2a)$$

$$I = \frac{J}{2mv} = \int_{l_1}^{l_2} \sqrt{1 - B/B_m} dl \quad (2b)$$

$$K \equiv \frac{J}{\sqrt{8m_0\mu}} = I_m \sqrt{B_m} = \int_{s_m}^{s_m'} [B_m - B(s)] ds \quad (2c)$$

where  $B$  is the local magnetic field strength and the subscript  $m$  refers to the mirror point. Note that lines of constant  $K$  correspond roughly to lines of constant magnetic latitude or  $B/B_0$ .  $K$  or  $I$  are generally preferred over  $J$  because they are independent of the particle energy.

The third adiabatic invariant  $\Phi$  captures the particle's drift motion:

$$\Phi = \oint A \cdot dx = \iint_{\pi} B_e \cdot dS \quad (3)$$

where  $A$  is the magnetic vector potential and the integral is carried out along a curve which lies in the particle drift shell [Roederer, 1970]. Alternatively, one can find the intersection of a series of drift shell field lines and compute the right-hand integral, where  $B_e$  is the magnetic field at the Earth's surface. Either way, calculating  $\Phi$  requires integration over an entire drift shell.

Although there are many advantages to using the adiabatic invariants, there are also several disadvantages. For example, use of the first invariant requires knowledge of the particle's pitch angle and the local magnetic field. The third invariant is very time consuming to calculate; this factor is one of the primary reasons for the popularity of McIlwain's  $L_m$  [McIlwain, 1961, 1966], since this parameter only requires the calculation of the second invariant. Finally, most work in the past has been done using quantities such as  $L_m$ ,  $B$ ,  $B/B_0$ , etc., and thus researchers in the field have developed an intuitive feeling for these parameters. Introducing a new coordinate system forces a change in thinking.

Finally, it should be noted that the adiabatic invariants are properties of the *particles*, not points in space. Different measurements taken at the same point in space may correspond to several different values of the adiabatic invariants depending on the particles' energies or pitch angles. Although we tend to treat the invariants as spatial coordinates, this distinction must be kept in mind. The same caution holds for dynamic conditions. A particle at a given location with a given energy and pitch angle will have a different set of adiabatic invariants under different magnetospheric conditions. Finally, because the invariants are functions of pitch angle, their advantages are reduced somewhat when dealing with omnidirectional data or integral-type detectors, which measure particles with a range of adiabatic invariants.

### 1.2.2.2 Other variables

In addition to the adiabatic invariants, some additional parameters are necessary either for improved mapping or to facilitate transforming to other coordinate systems for data analysis. The parameters calculated include:

- $h_{min}$ : This is defined as the minimum geodetic altitude on a drift shell and can be obtained as a by-product of computing  $\Phi$ .  $h_{min}$  provides excellent resolution at low altitudes where flux gradients are large. Appendix A discusses the relationships among  $K$ ,  $\Phi$ , and  $h_{min}$ . In addition, we also calculate the longitude of  $h_{min}$  (again in geodetic coordinates); this parameter may be useful in the future for better mapping of low-altitude electron data.
- McIlwain  $L_m$  and Roderer  $L^*$ : Calculating  $L_m$  and  $L^*$  enabled us to compare data with older data sets and helped provide an intuitive feel for the data. Note that  $L_m$  is computed using a constant value of the magnetic dipole parameter  $k_0$ :

$$k_0 = \frac{\mu_0 M_E}{4\pi} = 0.311653 \text{ G-R}_E^3 \quad (4)$$

- We did not generally compute  $L^*$  directly, but it can be calculated from  $\Phi$  using the relation

$$L^* = -\frac{2\pi k_0}{\Phi R_E}; \quad (5)$$

here, the preferred value of  $k_0$  is as given above, but it is common practice to use a value of  $k_0$  appropriate to the epoch of calculation.

- Magnetic Local Time (MLT): MLT is primarily of interest when mapping plasma fluxes.
- Local magnetic field strength  $B_{local}$  and equatorial magnetic field strength  $B_{min}$ . If the local pitch angle is known (or assumed to be  $90^\circ$ ), knowing  $B_{local}$  and  $B_{min}$  allows us to calculate the equatorial pitch angle  $\alpha_0$ .

It is impossible to measure most of the parameters discussed above, and in many cases quantities that can be measured (e.g.,  $B_{local}$ ) are not measured. Therefore, these parameters are calculated for all ephemeris points during the data processing and mapping phase. See Section 1.2.4 for a discussion of the calculation procedures.

### 1.2.2.3 Other considerations

In many circumstances the assumption of adiabatic invariance breaks down. For example, at low altitudes the particle flux is controlled more by the thermospheric neutral density than by the magnetic field; thus the flux is a function of altitude or density, and is also affected by the density variation over the solar cycle. Another factor is the difference between the drift loss cone and the bounce loss cone. Electrons in particular can be scattered onto drift shells which intersect the surface of the Earth at some point; as they drift westward eventually they are lost due to atmospheric interactions. Although these electrons are not permanently trapped, they are a persistent population and should be included in the trapped particle models. These and other factors were considerations in choosing coordinate systems for AE9/AP9/SPM.

### 1.2.3 Coordinates and Mapping Grids

As discussed in Section 1.2.2, the coordinates chosen for mapping fluxes in AE9/AP9/SPM are based on the adiabatic invariants. There is one exception to this rule: we have chosen to use energy instead of the first adiabatic invariant. Since energy is the quantity we want to use when accessing the flux maps, it makes sense to use it in creating the maps. Also, most detector channels measure a range of both energy and pitch-angle  $\alpha$ , making the spread of measured  $\mu$  much wider than just the spread in  $E$ .

Constructing the flux maps for AE9/AP9/SPM involved assigning individual flux measurements to bins within the map. These bins had to be small enough to provide adequate spatial resolution, yet large enough to contain a statistically significant number of measurements. In order to achieve the best possible resolution we chose to use two separate maps: a “global” map which covers essentially the entire region of interest, and a low-altitude map which provides greatly improved resolution at low altitudes and near the loss cone.

The global grid for mapping both proton and electron fluxes is based on the second and third adiabatic invariants  $K$  and  $\Phi$ . Transforming these variables into  $K^{1/2}$  and  $\log_{10}(\Phi)$  improves resolution near the magnetic equator (small values of  $K$ ) and at large values of  $\Phi$ .

Even with these transformations, however, resolution is still poor near the loss cone. Therefore a low-altitude grid was added. This grid uses  $K^{1/2}$  and  $h_{min}$ .

The plasma model SPM uses a different coordinate system based on the equatorial pitch angle and McIlwain  $L$ .

For AP9/AE9/SPM version 1.0, the coordinate grids are given in Table 1.

**Table 1. AE9/AP9/SPM coordinate grids.**

Model	Species	Energy	High Altitude Grid		Low Altitude Grid	
			2 <sup>nd</sup> Inv.	3 <sup>rd</sup> Inv.	2 <sup>nd</sup> Inv.	3 <sup>rd</sup> Inv.
AE9	e-	0.04-10 MeV 21 channels	$0 \leq K^{1/2} \leq 4.5$ $\Delta(K^{1/2}) = 0.1$	$-0.8 \leq \log_{10}\Phi \leq 0.3$ $\Delta(\log_{10}\Phi) = 0.025,$	$0 \leq K^{1/2} \leq 4.5$ $\Delta(K^{1/2}) = 0.1$	$-500 < h_{min} < 1000$ km $\Delta h_{min} = 50$ km
AP9	H+	0.1-400 MeV 22 channels	$[K] = G^{1/2}R_E$	$[\Phi] = G R_E^2$	$[K] = G^{1/2}R_E$	$0 < h_{min} < 1000$ km $\Delta h_{min} = 50$ km
SPME	e-	1-40 keV 16 channels	$5 \leq \alpha_{eq} \leq 85^\circ$ $\Delta\alpha_{eq} = 10^\circ$	$2 \leq L_m \leq 10$ $\Delta L_m = 0.5$	N/A	
SPMH	H+	1.15-164 keV				
SPMHE	He+	12 channels				
SPMO	O+					

Figure 1 shows the 1 MeV median flux from the AE9 model mapped in the two grids. In Figure 1a the y-axis ( $K=0$ ) is the magnetic equator, and the loss cone is the boundary with the white region, where fluxes are zero. The inner and outer zones are clearly visible as regions of high flux centered at  $\log_{10}\Phi$  values of about 0 and -0.4, respectively, with the slot region in between. The dashed gray diagonal curves indicate the locations of two  $h_{min}$  contours; the curve to the upper right corresponds to  $h_{min}=0$  km, and the curve to the lower left corresponds to  $h_{min} = 1000$  km, which is the upper boundary of Figure 1b. Also shown in the figures are contours of the traditional ( $L_m, B/B_0$ ) coordinates (used in the AP8/AE8 and CRRES models, for example). It can be seen from Figure 1b that using  $h_{min}$  as a coordinate gives much better resolution of the fluxes at low altitudes (or near the loss cone) where the neutral density and consequently altitude becomes a dominant ordering parameter.

While the two grids described above account for secular changes in the Earth's magnetic field, they do not account for changes due to the solar cycle. It has been shown that the particle flux at low altitudes is a function of the thermospheric density [Huston *et al.*, 1996]. We attempted to develop a parameter which would account for the changes in the thermospheric density and thus enable a true solar cycle variation in the particle fluxes. However, no simple function gave results which were significantly better than  $h_{min}$  alone. An approach similar to that taken in TPM-1 [Huston, 2002], in which the solar cycle variation for a given ( $E, K, h_{min}$ ) is correlated with the solar  $F_{10.7}$  flux, may be possible, but at this point there is not sufficient data to implement this approach for all energies. The variation in flux from AE9 or AP9 that is obtained using either the perturbed or Monte Carlo methods does include the variation due to solar cycle effects, but there is no explicit dependence on the solar cycle phase.

The use of two grids poses no problem for mapping the fluxes; measured fluxes at each ephemeris point are simply mapped to both grids. The procedure for accessing the flux maps is also fairly straightforward. For a given location and local pitch angle  $\alpha$ , we first check to see if the point is in the  $K/h_{min}$  grid. If not, we check to see if it's in the  $K/\Phi$  grid. The two grids overlap slightly, and the  $K/h_{min}$  grid takes precedence.

However, to integrate over local pitch angle  $\alpha$  to obtain an omnidirectional flux, we must interpolate from both the  $K/\Phi$  and  $K/h_{min}$  grids onto an  $\alpha$  grid. The procedure is illustrated in Figure 2. The integral is defined as:

$$J = 4\pi \int_0^{\pi/2} j(\alpha) \sin \alpha d\alpha = \sum_i w_i j(\alpha_i) = \sum_i w_i \begin{cases} j(K(\alpha_i), h_{min}(\alpha_i)) \\ j(K(\alpha_i), \Phi(\alpha_i)) \end{cases} \quad (6)$$

The  $w_i$  represent the combined weights for numerical integration and linear interpolation. We interpolate from the blue circles/squares to the black points ( $K/\Phi$  or  $K/h_{min}$ ) at the fiducial  $\alpha_i$ : 5, 10, 20, ..., 90). **The integral in  $\alpha$  is evaluated** assuming linear interpolation of flux between the black points. The upper right black point is in the loss cone and its flux is set to zero (i.e., it will be left out of the integrals implicitly). Section 1.3.5.2 discusses how interpolation within and across grids is performed.

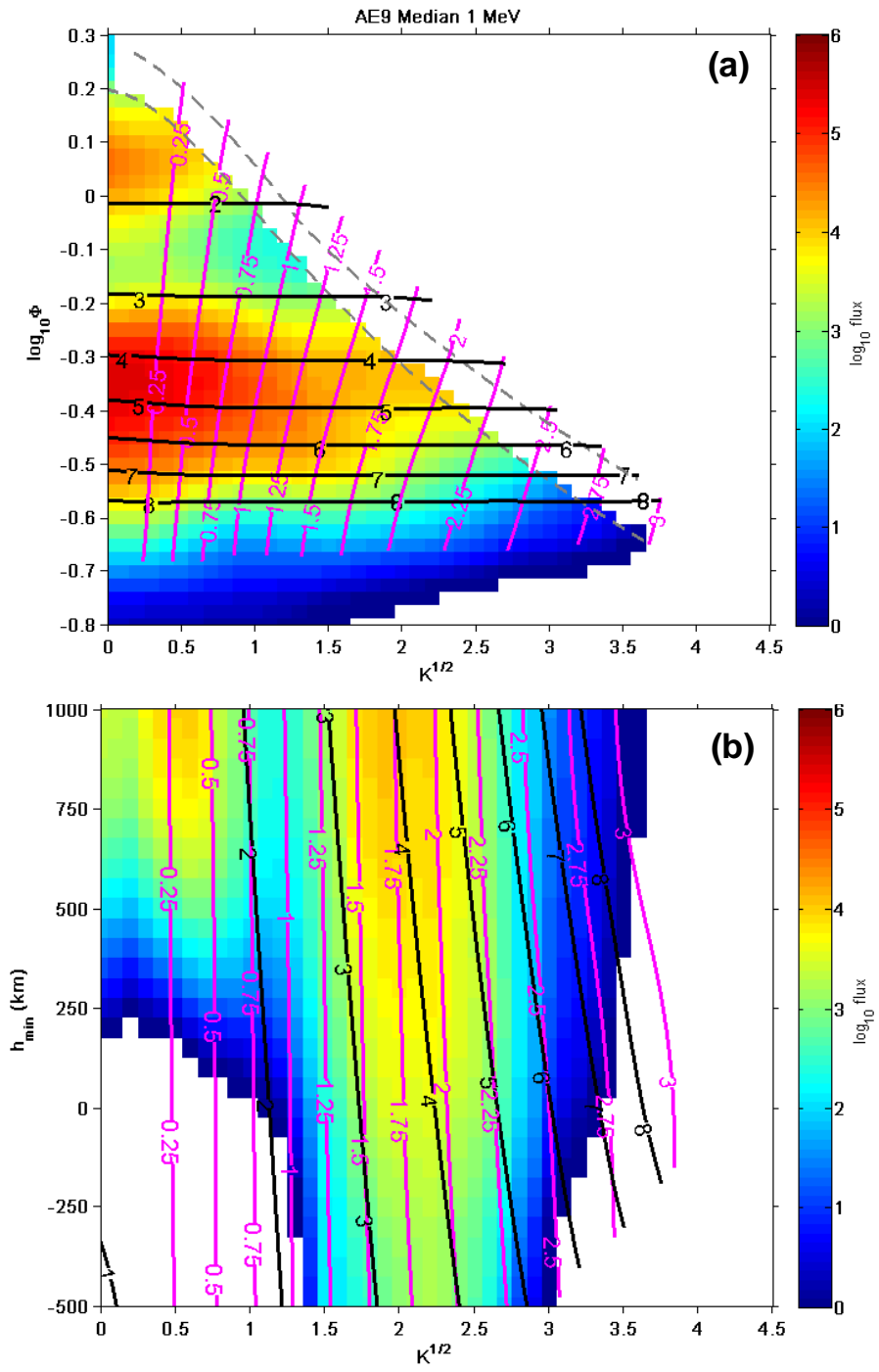


Figure 1. 1 MeV electron flux from AE9 plotted in two coordinate systems.

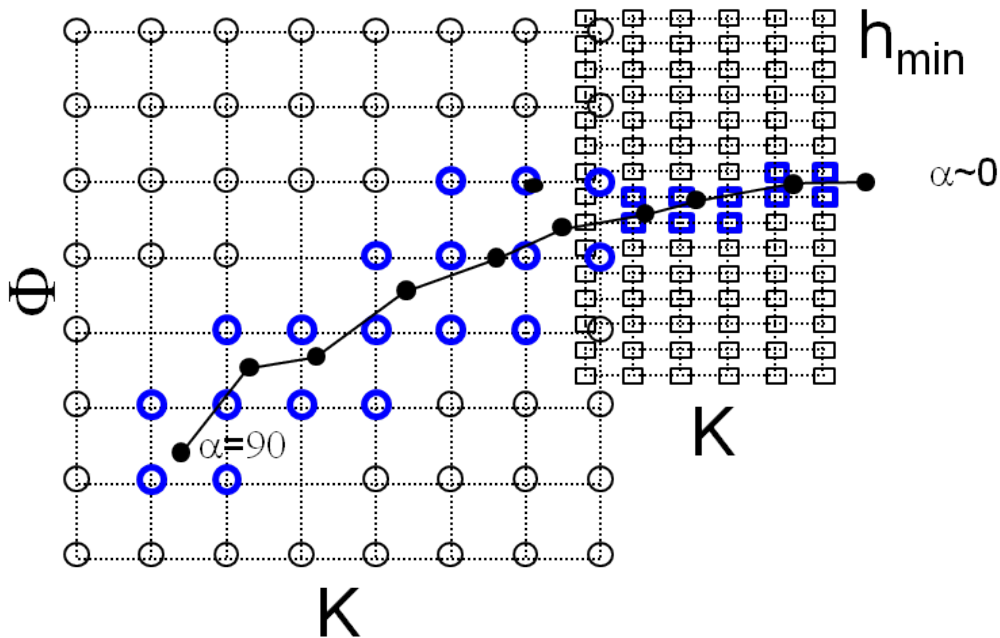


Figure 2. Procedure for integrating over local pitch angle to obtain omnidirectional flux.

## 1.2.4 Calculation Procedures

There are two types of coordinate calculations: those performed to map the data into the model, and those performed to access the model maps when the user invokes the model.

### 1.2.4.1 IRBEM-LIB

For processing ephemerides of individual data sets, IRBEM-LIB [IRBEM, 2012] was used. Ephemeris data (latitude, longitude, altitude, universal time) were input, and the parameters listed in Section 1.2.2 were output. The original version of IRBEM-LIB was modified to calculate  $h_{min}$  as well as  $\Phi$  and to perform the calculation even if the drift shell dipped below the surface of the Earth. This modification was required in order to account for particles (primarily electrons) which are within the bounce loss cone but not necessarily in the drift loss cone.

The invariants were calculated for a range of pitch angles between  $10^\circ$  and  $90^\circ$ . For pitch angle resolved data, the invariants were interpolated to the correct pitch angle.

### 1.2.4.2 Magnetic field model

For all coordinate and mapping calculations, the Olson-Pfitzer Quiet Magnetospheric magnetic field model (OPQ77) [Olson and Pfitzer, 1977] was used. The OPQ77 model represents all major magnetospheric current systems and is valid for all tilt angles; i.e., angles of incidence of the solar wind on the dipole axis. OPQ77 has been shown to be a good average model for the inner magnetosphere [Jordan, 1994; McCollough et al., 2008]. The model accurately represents the total magnetospheric magnetic field for conditions of low magnetic activity and to a geocentric distance of 15 Earth radii or to the magnetopause.

Although the data used in AE9/AP9/SPM were taken at all levels of magnetospheric activity, it was decided that using an activity-dependent model would be inappropriate for the model maps. If an activity-dependent model were used to map the data, the same model would be required to “un-map” the data when using the model. Since a user would not know *a priori* what the activity level would be over the course of a future mission, using such a model would not have any practical benefit. Therefore, any error associated with calculating the mapping coordinates is combined with the measurement errors in the flux maps.

The OPQ77 external field model was combined with the IGRF model [Langel, 1991; Finlay *et al.*, 2010; IGRF, 2012] appropriate to the epoch at which the measurements were taken.

### **1.2.4.3 Neural network**

Calculation of the drift shells needed to evaluate  $\Phi$  and  $h_{min}$  is a very time-consuming process. Direct computation with the IRBEM-LIB routines was sufficient for construction of the flux maps since there are a relatively small number of ephemerides to compute. By contrast, the computational load to convert the flux map coordinates can quickly become unrealistic in the general application, where a user might evaluate many orbits for long periods of time. A neural network interpolation algorithm was therefore developed to produce  $\Phi$  and  $h_{min}$  without the computational expense of integrating over an entire drift shell. For a given satellite position and detector look direction the inputs include the Universal Time (UT), day of year, modified Julian day,  $I (=K/\sqrt{B})$  and  $B_m$  thus requiring a trace of the field line only. The neural network is an integral part of the AE9/AP9/SPM software allowing  $\Phi$  and  $h_{min}$  to be calculated almost as quickly as  $L_m$ . The algorithm is augmented with boundary models that specify the location of the loss cone at low altitudes and the onset of Shabansky or open drift orbits at high altitudes. The neural network is described in more detail in Sections 1.5 and 1.3.5.1.